Differential Lung Proteome Profiles Upon Pulmonary Exposure to Traffic-related Particulate Matter

Yu-Teng Jheng
Taipei Medical University
Denise Utami Putri
Taipei Medical University
Hsiao-Chi Chuang
Taipei Medical University
Kang-Yun Lee
Taipei Medical University
Hsiu-Chu Chou
Taipei Medical University
San-Yuan Wang
Taipei Medical University
Chia-Li Han (was@tmu.edu.tw)
Taipei Medical University https://orcid.org/0000-0003-4644-5892

Research

Keywords: Traffic-related air pollution, particulate matter, lung injury, proteomics

Posted Date: July 10th, 2020

DOI: https://doi.org/10.21203/rs.3.rs-40838/v1

Abstract

Background: Exposure to particulate matter (PM) pollution has direct impacts on the respiratory organs, yet the molecular alterations underlying PM-induced pulmonary injury remain unclear. In this study, we investigated the effect of PM on lung tissues from our previously reported rat model with whole-body exposure to traffic-related PM_1 pollutants and compared it with rats exposed to high-efficiency particulate air-filtered gaseous pollutants and clean air control for 3 and 6 months. Lung function and histological examinations as well as quantitative proteomics analysis and functional validation were performed.

Results: The rats in 6-month PM_1-exposed group showed significant decline in lung function by decreased forced expiratory flow and forced expiratory volume, but the histological analysis revealed an earlier lung damage evidenced by increased congestion and macrophage infiltration in 3-month PM_1-exposed rat lungs. The lung tissue proteomics analysis identified 2,673 proteins which highlighted dysregulations on proteins involved in oxidative stress, cellular metabolisms, calcium signaling, inflammatory responses, and actin dynamics. The presence of fine particles specifically enhanced the oxidative stress and inflammatory reactions under sub-chronic exposure of traffic-related PM_1 and suppressed the glucose metabolism and actin cytoskeleton signaling which might lead to repair failure and thus lung function decline after chronic exposure of traffic-related PM_1. A detailed pathogenic mechanism was proposed to depict the temporal and dynamic molecular regulations associated with PM_1-induced lung injury.

Conclusion: Our study explored the earlier lung injury prior to lung function decline and proposed several proteins as potential molecular features for traffic-related PM_1-induced lung injury.

Background

Ambient air pollution contributes substantially to major disease burden as well as mortality globally, with at least 4.2 million reported deaths in 2016 (1). Among various pollutants in ambient air pollution, exposure to particulate matter (PM), particularly in the fine ($PM_{2.5}$) and ultrafine ranges ($PM_{0.1}$), is considered as a key risk factor for many adverse health consequences of which acute or chronic respiratory complaints are prominently reported due to a direct deterioration in the organs upon inhalation of air pollution (2, 3). Short- or long-term exposure to fine PM air pollution would significantly reduce the lung function with increased pulmonary oxidative stress and persistent inflammation (4-7). Multiple signaling pathways involved in the transcriptional and/or translational activations of AMP-activated protein kinase (AMPK)/signal transducer and activator of transcription (STAT)-1 (8), epithelial growth factor receptor (EGFR)/mitogen-activated protein kinase (MAPK)/ nuclear factor κB (NF-κB) (9), and transforming growth factor (TGF)-β/Smad (10) that promote the release of pro-inflammatory cytokines were proposed on lung epithelium cells or rodent models as potential pathogenic mechanisms of the PM-induced pulmonary toxicity. However, the detailed pathogenesis behind remains to be fully investigated.

Mass spectrometry (MS)-based proteomics analysis that enables unbiased identification and quantification of thousands of proteins has been applied to study the aberrant molecular profiles upon PM-induced damages on primary skin keratinocytes (11), trophoblast cells (12), lung epithelial cells (13), rat lung (14) and rat brain (15). Several dysregulated proteins involved in mitochondria dysfunction, energy metabolism and ER stress were discovered as potential biomarkers for PM-induced organ damage. To exploit the impact of PM on organ injury, we have previously established the rat model with whole-body exposure system and reported the central neurotoxicity induced by sub-chronic or chronic exposure of traffic-related fine PM (PM_1), even though it was below the WHO air quality guideline (16). In this study, we aimed to investigate the effects of traffic-related PM_1 in lungs from the same rat model. Specifically, we elaborated the lung function and pathological changes upon sub-chronic or chronic exposure of traffic-related PM_1 as well as systematically elucidated the dysregulated molecules and signaling pathways by using quantitative proteomics analysis to construct the molecular mechanisms underlying traffic-related PM_1-induced lung injury.

Results

Lung function and histological examination

We examined the lung function of each rat by measuring the forced expiratory flow at 25-75% of the pulmonary volume (FEF_{25-75}) and forced expiratory volume at 20 ms (FEV_{20}). As shown in **Fig. 1**, there was no significant differences in FEF_{25-75} and FEV_{20} among rats in the 3-month exposure groups. After 6-month exposure rats in PM_1 group showed significant decrease in FEF_{25-75} and FEV_{20} in comparison to both GAS and CTL rats. We also evaluated the degree of lung injury based on the presence and severity of congestion, hemorrhage, immune cell infiltration, and thickness of the alveolar wall using the lung histological analysis. The 3-month PM_1-exposed lungs already exhibited higher levels of congestion and macrophage infiltration, indicating a significant lung injury in PM_1 rats compared to GAS and CTL rats. Similar results were observed after chronic exposure to PM_1 (**Table 1**). **Fig. 2** showed the histological images demonstrating the increased thickness of airway wall and disruption of alveolar and airways integrity, along with abundant immune cell accumulation within the peribronchial area in both 3-month and 6-month PM_1-exposed lungs. However, no significant difference in lung jury was observed between rats under 3-month and 6-month exposures.

Quantitative proteomics analysis of rat lungs

In order to elucidate the molecular mechanisms underlying traffic related air pollution (TRAP)-induced lung injury, we applied the tandem mass tag (TMT)-based quantitative proteomics analysis on the lung tissues from the 6 exposure groups. As shown in **Fig. 3A**, five rats were randomly selected from each group to collect the lung tissue lysate and perform gel-assisted digestion with trypsin individually. Peptides from the same group of rats were pooled and labeled with one of the TMT tags. All the TMT-labeled peptides were combined for high-pH reversed phase (RP) StageTip fractionation and each

fraction was analyzed in duplicate by LC-MS/MS, followed by proteome identification and quantification using Proteome Discoverer. A total of 2,673 proteins were confidently identified (p<0.05, FDR<1%) of which 2,562 proteins were quantified (**Fig. 3A**).

In the present study, we arranged our analyses in three directions and considered proteins with 1.3-fold change (log2 ratio >0.38 or <-0.38) in abundance in two comparisons as differentially expressed proteins (DEPs). (1) We aimed to observe the sub-chronic effect of TRAP by comparing the protein expressions in 3-month (3M) exposure of GAS and PM_1 groups to the clean-air CTL group which generated 218 and 179 DEPs in the 3M-GAS and 3M-PM_1 groups, respectively. (2) The proteins associated with progressive lung injury when exposed to GAS and PM_1 were studied by comparing the protein expressions between 6- and 3-month exposures on each GAS and PM_1 groups. A total of 408 and 413 progression-associated DEPs were identified in GAS and PM_1 groups, respectively. (3) We elucidated the particle-specific regulations by comparing the PM_1 to GAS under sub-chronic (3-month) and chronic (6-month) exposures, which resulted in 119 and 103 DEPs in 3M and 6M comparisons, respectively (**Fig. 3B**). The DEPs were listed in **Additional file 1-3: Table S1-3** and were further analyzed by using Gene Ontology (GO) and IPA (Ingenuity pathway analysis) to delineate the dysregulated cellular functions and pathways in lungs.

Dysregulated cellular functions and pathways in rat lungs under sub-chronic and chronic exposure to GAS and PM_1 pollutants

As shown in **Additional file 4: Figure S1**, 3-month exposure to traffic related air pollution (TRAP)-related gaseous and PM_1 pollutants induced alterations in proteins involved in metabolism- and acute phase response-related biological processes. Upregulation of arginine metabolic process and fatty acid beta-oxidation, as well as down-regulation of endopeptidase inhibitor activity and negative regulation of mRNA metabolic process were enriched in 3M-GAS group (**Additional file 4: Figure S1A**). Similarly, sub-chronic exposure to PM_1 up-regulated triglyceride catabolism, reactive oxygen species (ROS) metabolism, long-chain fatty acid metabolism, and down-regulated glycolytic process within lung tissues (**Additional file 4: Figure S1B**). It is noted that 3M-GAS group exhibited down-regulation of immune-related functions, including negative regulation of CaN-NFAT signaling cascade, blood coagulation and complement activation (classical pathway). Meanwhile the 3M-PM_1 group regulated processes related to tissue damage and wound healing, such as ATP biosynthesis, ROS metabolism, regulation of wound healing and DNA geometric change. The DEPs in both 3M-GAS and 3M-PM_1 groups were enriched as mitochondrial membrane proteins. Additionally, the 3M-PM_1 group enriched proteins localized in sarcoplasmic reticulum (**Additional file 4: Figure S1**). Pathway analysis of the DEPs suggested common up-regulation of oxidative phosphorylation and inositol phosphate metabolism and down-regulation of sirtuin signaling pathway in both 3M-PM_1 and 3M-GAS groups (**Fig. 4**). The glycolysis and gluconeogenesis pathways were enriched in both groups as well, but showing inhibition in only 3M-GAS group. Inflammation related pathways, including acute phase response signaling and mTOR signaling, were activated exclusively in 3M-PM_1 group, while complement system and acute phase response signaling were inhibited in 3M-GAS group. Altogether, our results indicated that exposure to TRAP induced

early metabolic changes. Sub-chronic PM_1 exposure promoted more acute phase responses within the lung tissue, while exposure to gaseous pollutant showed more suppression on the complement system.

We next analyzed the injury progression-related biological process within the lung tissue. As shown in **Additional file 5: Figure S2**, we observed several tissue development and wound healing related processes in both GAS- and PM_1-exposed rats. The DEPs involved in inflammatory response and metabolism processes were also enriched. The cellular component mapping pointed out that DEPs located in extracellular vesicle and plasma membrane were upregulated, while cytosolic proteins were prominently downregulated in both groups. The pathway analysis result in **Fig. 4A** showed exclusive inhibition of inositol phosphate metabolism pathways in lung tissues upon prolonged exposure to GAS pollutant. The glycolysis I pathway was up-regulated in GAS group but down-regulated in PM_1 group. Inflammatory pathways including acute phase response signaling and complement system were exclusively enriched in PM_1 group, yet the net effect is not clear. In addition, we observed some common pathways including activated G Beta Gamma and calcium signaling as well as inhibited protein kinase A, EIF2 signaling and LXR/RXR activation in both GAS and PM_1 groups. Interestingly, exposure to GAS pollutants uniquely enriched progressive up-regulation of pathways related to actin cytoskeleton and Rho family GTPases signaling which involve in cell migration, muscle contraction and potentially tissue repair.

Regarding the particle-specific effects, the GO analyses suggested that the fine particles in the present study prominently up-regulated the endopeptidase inhibitor activity and humoral immune response in the sub-chronic exposure stage, while blood coagulation was continuously activated upon prolonged exposure (**Additional file 6: Figure S3**). Furthermore, the particles down-regulated proteins located in chromosome under sub-chronic exposure, while later at 6 months of exposure, downregulated proteins localized within the A band of the muscle fiber were noticed (**Additional file 6: Figure S3**). Pathway analysis indicated that during sub-chronic exposure, the particles in the TRAP specifically induced greater inflammatory reactions through LXR/RXR activation, acute phase response signaling, and complement response (**Fig. 4B**). Upon prolonged exposure, the particles inhibited glycolysis and gluconeogenesis as well as ILK and actin cytoskeleton signaling when compared to the GAS group. In summary, from 3 to 6 months of PM_1 exposure, we observed an early induction of inflammatory reactions and a progressive reduction in the glucose metabolism and cell movement functions.

Proposed molecular mechanisms underlying PM_1-induced lung injury

Based on the functional analysis results, we proposed a detailed molecular mechanism in **Fig. 5**. The expression changes of DEPs were displayed by using the boxes that surrounded the protein gene symbol. Boxes on the upper side of the protein gene symbol indicate the protein expression in PM_1 (upper) and GAS (lower) groups. Boxes on the left panel of upper side showed the protein ratios in 3M-PM_1/CTL and 3M-GAS/CTL, while those on the right panel represented a progression from 3- to 6-month exposures (PM_1-6M/3M and GAS-6M/3M, respectively). Upregulated proteins were marked in red, downregulated proteins in green, while unchanged proteins were shown in white color. We also indicated the particle-

specific regulations in both 3 (left panel) and 6 months (right panel) of exposures in boxes in the right side of the protein gene symbol (3M-PM_1/GAS and 6M-PM_1/GAS, respectively). Protein expressions enhanced by particles was presented with fuchsia color, while suppression was in cyan color.

Firstly, we highlighted the dysregulated proteins and pathways involved in acute phase response signaling during the sub-chronic exposure to traffic-related GAS and PM_1; Ras/Erk to NF-IL6 pathway, Ras/Pi3k/Akt to Nf-κB pathway, Il-6 to Stat3 pathway, and Tcf transcriptional regulations showed differential expressions in both 3M-GAS and 3M-PM_1 rats (**Fig. 5**, pathways in blue color). It is noted that proteins responding to oxidative stress, including Ttr (compared to 3M-CTL), Cp, and Hmox2 (compared to 3M-GAS), as well as the inflammatory related proteins (Itih3, Serpina3, Fga and Hpx) within the acute phase response pathways were up-regulated in 3M-PM_1 group. In addition, the presence of particles specifically up-regulated complement proteins (C3, C4, C5 and C1q) in comparison to 3M-GAS group.

The mTOR complex which responds to stress and regulates cellular metabolism, cell growth and survival was dysregulated under sub-chronic PM_1 exposure (**Fig. 4A**, **Fig. 5**, pathway in purple color). In response to PM exposure, mTOR has been reported to be activated in macrophage (17) or suppressed in airway epithelium (18), where it both showed protective effect against lung injury by attenuation of inflammatory responses and cell death. In the present study, we observed up-regulated mTOR pathway, in particular the mTORC2 complex with upregulation of mTor and down-regulation of Mapkap1 and inhibitory Tsc2 under the sub-chronic exposure to PM_1, suggesting potential protection and homeostasis effect to minimize lung injury. Furthermore, the up-regulated Ras/Raf/Mek/Erk signaling promoted Eif2 signaling through up-regulation of Ppp1c and Eif2b3 proteins (**Fig. 5**, pathways in grey color). However, this pathway was gradually down-regulated under prolonged exposure to both GAS and PM_1 with concurrent decrease in the 40S and 60S ribosomal protein complexes which resulted in reduced protein synthesis and enhanced apoptosis (19).

Secondly, we highlighted the dysregulation of calcium signaling cascade in PM_1-induced injury progression (**Fig. 5**, pathways in orange color). In our data, multiple signallings that evoke the regulation of intracellular calcium ion (Ca^{2+}) showed differential expressions. The inositol 1,4,5-trisphosphate (IP3) pathway was triggered by progressive elevation of G protein couple receptor (represented as Gβ4)/phospholipase C (Plcb2) signaling to release the Ca^{2+} from endoplasmic reticulum to mitochondria and lysosome which further regulated metabolic processes. The progressive up-regulation of sarco/endoplasmic reticulum Ca^{2+}-ATPase (shown as Atp2a1) and down-regulation of ryanodine receptor (Ryr1) suggested a re-storage and inhibited release of Ca^{2+} from sarcoplasmic reticulum to cytoplasm in the cell. In addition, we observed the upregulations of intracellular calcium-binding Camk2g (calcium/calmodulin-dependent protein kinase type II subunit gamma) as well as inhibitory Chp1 (Calcineurin B homologous protein 1) and Akap5 (A-kinase anchor protein 5) proteins that suppress the calcium-dependent calcineurin phosphatase activity for calcium homeostasis control. According to these results, we speculated an accumulation of intracellular Ca^{2+} in rat lungs which might promote lymphocyte activation during injury progression.

Thirdly, proteins involved in RhoA/Rock-, Rac- and Cdc42-mediated signalings for controlling the muscle contraction, actin dynamics, and cell migration were also impaired during the progression of lung injury (**Fig. 5**, pathways in green color). Interestingly, we observed an unbalanced activation of these three pathways in the PM_1 rats. The RhoA/Rock pathway activated via Gb4/Gai2 and mTORC2 ultimately up-regulated Acta2, myosin 11 (Myh11), and tropomyosin (Tpm2, 5, 12) complex which increased the contractility in lungs of both GAS and PM_1 rats. However, the Rac- and Cdc42 pathways were activated only in GAS rats through up-regulation of Cd14, Arhgef, Apc, Acta2 and down-regulation of inhibitory Tmsb4 and Ssh3 proteins which promoted actin polymerization and stabilization and subsequent cell migration. These results suggested an activation of myosin-axis contraction but absence of actin dynamics under the prolonged exposure of traffic-related PM_1.

Functional validation

Among the discovered DEPs, we selectively validated the expression levels of inflammatory related proteins, C3, Chp1, and Serpina3, in rat lungs by using western blotting. The representative images were shown in **Additional file 7: Figure S4**. The statistical result in **Fig. 6A** showed that C3 were significantly upregulated in 3M-PM_1 group compared to 3M-GAS group while no significant difference was observed in 6M exposure groups. Serpina3 showed significantly higher expressions in 3M-PM_1 group and slightly higher expression in 6M-PM_1 groups in comparison to the corresponding GAS groups (**Fig. 6B**). The inhibitory Chp1 protein exhibited up-regulation in only 3M-GAS group. Additionally, we investigated the oxidative stress and inflammatory profiles within lung tissue by measuring 8-isoprostane and IL-6 using ELISA assays, respectively. The data revealed a higher level of oxidative stress in both 3M-GAS and 3M-PM1 groups while only 6M-GAS group showed higher oxidative stress compared to CTL group (**Fig. 6D**). Interestingly, the rat lungs exhibited higher level of IL-6 in 3M-PM1 group in comparison to GAS and CTL groups while there was no significant difference in IL-6 level between 6M-PM_1 and 6M-GAS groups (**Fig. 6E**). These results suggested an earlier oxidative stress and inflammatory reaction in 3-month PM_1-exposed rats which was in consistent with the proteomics data.

Discussion

Epidemiological studies reported that prolonged exposure of PM is associated with the declined lung function (20, 21), yet the detailed molecular mechanism remain unclear. Thus, we aimed to investigate how the traffic-related PM_1 impacts on lungs in our previously reported rat model (16). In the present study, we observed statistically significant decline of lung function with decreased FEF_{25-75} and FEV_{20} after 6 months of pulmonary exposure to traffic-related PM_1. On the other hand, the histological examination of the lung tissues showed a significant lung injury under sub-chronic (3-month) exposure of PM_1, as characterized by increased level of congestion and macrophage infiltration in the lung tissues (**Table 1**). These results suggested that the presence of PM caused earlier lung damages prior to lung function decline under the pulmonary exposure to traffic-related PM_1, even though the overall air quality was under the WHO guideline. Other study in rats exposed to biomass fuel and motor-vehicle exhaust

pollutants also showed increased leukocyte counts in bronchoalveolar lavage and accumulated inflammatory cells within the airway walls as early as one to three months of exposure, while the significant reduction of lung functions were only observed at 7 months of exposure (7).

In order to elucidate the underlying mechanism, we systematically studied the perturbed function and pathways underlying lung injury upon sub-chronic and chronic exposure of traffic-related PM_1 by using MS-based quantitative proteomics analysis (**Fig. 3, 4 and Additional file 4-6: Figure S1-3**). The functional analysis revealed early dysregulations on lipid, glucose and protein metabolism, acute phase response signaling and complement system which may directly or indirectly contribute to the lung injury under the sub-chronic exposure of PM_1. While the injury progressed, the metabolic pathways were down-regulated while the tissue repair and wound healing related functions and pathways were activated, especially in rats in the GAS group. Nevertheless, the rats in 6M-PM_1 group showed significant lung function decline by decreased FEV_{20} and FEF_{25-75} which might be due to the failure on triggering wound healing-related pathways. Our data also suggested that the presence of ultrafine-sized particles specifically enhanced the inflammatory reactions during sub-chronic exposure as well as inhibited the glucose metabolism and actin cytoskeleton signaling after chronic exposure. The temporal and dynamic proteome changes observed in the present study highlighted a complex regulation at the cellular and molecular levels in lungs caused by traffic-related PM_1 pollutants.

Fine and ultrafine PMs have been reported to induce lung diseases through generation of ROS and oxidative stress as well as activation of innate and adaptive immunity, leading to cell barrier and tissue damage (22, 23). Several known promoters of inflammatory response, such as nuclear factor-κB (NF-κB), activation protein-1 (AP-1), nuclear factor erythroid 2 related factor 2 (Nrf2), and CREB-binding proteins (CBPs), are activated by oxidative stress (24-26). In our study, we observed significantly higher levels of oxidative stress and IL-6 in together with up-regulation of inflammation-related pathways including acute phase response and complement system in rats exposed to PM_1 for 3 months. As a key component in innate immune system, both pathogen infection and tissue damage would trigger the complement system which further promotes chemotaxis (27), activates neutrophil and macrophage for chemokine secretion (28), and exacerbates acute lung injury through autophagy-mediated alveolar macrophage apoptosis (29). Walters *et al.* reported that $PM_{2.5}$-treated mice underwent airway hyper-responsiveness resulted from the activation of C3 (30). In adults with age above 65 years in China, short-term exposure to $PM_{2.5}$ resulted in a significant increase in serum complement C3 and inflammatory reaction (31). The ultrafine-sized PM ($PM_{0.1}$) enhanced pulmonary inflammation by rapid influx of neutrophils and pro-inflammatory cytokine secretion (32). Moreover, smaller size of PM induced higher IL-6 release from A549 cells compared to coarse particles (33), pointing out the threat of smaller particles, which can penetrate deep into the respiratory tract and absorbed by the blood stream (34). These findings support that the prompt attack of the fine particles in our rat model elevated the oxidative stress in lung and promoted the higher infiltration of immune cells, contributing to activation of acute phase signaling pathways and complement system and thus the significant lung injury in 3M-PM_1 rats (**Table 1** and **Fig. 2C**). However, it is noted that proteins involved in complement system and the acute phase response signaling did not

show significant changes upon chronic PM_1 exposure in our rat model. Thus, we speculated that the acute phase response signaling and complement activation may be the early events mediating pulmonary inflammation upon PM_1 exposure. These early inflammatory responses to PM_1 could be characterized as unique molecular features in sub-chronic stage of lung injury.

The infiltration of PM in lung is known to disrupt the cell membrane integrity and subsequently increase the intracellular calcium ion (Ca^{2+}) concentration. The calcium signaling affects a broad spectrum of cellular functions such as motility, metabolism, cell growth, proliferation and apoptosis (35) and the dysregulation of intracellular Ca^{2+} has been reported to associate with PM-induced oxidative stress and inflammation in human lung fibroblast cells (36), pulmonary artery endothelium cells (37), and mouse lungs (38). Proteins that control efflux and influx of calcium stand important roles in calcium homeostasis. In cystic fibrosis, the decreased expression and activity of SERCA were observed to increase susceptibility of airway epithelium cells to oxidant gas exposure and cell death (39, 40). In our model, we observed dysregulation of IP3-, SERCA- and calmodulin/calcineurin-mediated calcium signalings. Among the involved DEPs, SERCA (as Atp2a1, sarcoplasmic/endoplasmic reticulum calcium ATPase 1) was inhibited in both 3M-PM_1 and 3M-GAS groups, probably as an early response to TRAP. It was later upregulated in both 6M-PM_1 and 6M-GAS rats in together with the lower expression of Ryr1, which could be an attempt to limit the Ca^{2+} leak from sarco/endoplasmic reticulum and balance the elevated cytoplasmic Ca^{2+} concentration. The high intracellular Ca^{2+} concentration were also reported to promote NFATc signaling and subsequent activation of lymphocyte (41), demonstrating its role as pro-inflammatory mediator. Despite of the biological significance of calcium signaling in lung injury, how these dysregulated calcium signalings coordinately contribute to PM-induced oxidative stress, metabolism, and inflammation remain unclear. More cellular and molecular studies are required to address these issues.

Furthermore, the accumulation of Ca^{2+} in the cytoplasm may serve as a signal for initiation of wound healing in the injured rat lungs (42). Wound healing and tissue repair are a multi-step process composed of wound sensing and blocking, plasma membrane restorage, and cytoskeleton remodeling. Although the detailed wound healing mechanism is not clear yet, it is reported to be tightly controlled by Rho family GTPase pathways, including RhoA/Rock, Rac and Cdc42 signalings (43-45). In our model, the Rhoa/Rock-mediated actomyosin contraction was activated in response to the prolonged exposure to PM_1 by the upregulated Ga4, Itgb1, Cd14 proteins and the increased levels of intracellular Ca^{2+} and mTORC2 complex, suggesting a repair initiation for membrane resealing and wound closure. However, the Rac and Cdc42 signalings were not activated in PM_1 rat, making it unable to trigger actin polymerization and stabilization for cytoskeleton remodeling (46) and thus limit the tissue repair potential and ultimately lead to the declined lung function. The concomitant up-regulation of these Rho family GTPase-mediated pathways was exclusively observed in the GAS-exposed rats, highlighting the role of PM in disrupting the repair potential. On the other hand, the progressive upregulation of the actin, myosin, and tropomyosin protein complexes in the PM_1 rats may represent the increased quantity of

smooth muscle as observed on the thickening of the airway wall, or a possible fibrosis formation within the lung tissue (47).

Although not included in **Fig. 5**, both GAS and PM_1 pollutants stimulated alterations on metabolic pathways, notably on oxidative phosphorylation, lipid (inositol phosphate superpathways) and glucose (glycolysis/gluconeogenesis) metabolism. Increased oxidative phosphorylation was observed in both 3M-PM_1 and 3M-GAS groups which may imply impaired mitochondrial functions, higher oxidative stress (48) and probably a compensation of metabolic shifting from glycolysis to pentose phosphate pathway (49). Glycolysis was reported to worsen infection related-pulmonary fibrosis (50), and inhibition of glycolysis would attenuate the injury by suppressing inflammation and apoptosis (51, 52). Concurrently, our model showed negative regulation of glycolysis/gluconeogenesis in chronic PM_1-exposed rats, suggesting a potential mechanism to limit lung injury. Regarding the lipid metabolism, a recent metabolomics study reported that an organic component of $PM_{2.5}$, benzo[a]pyrene, would induce lung injury by altering lipid metabolism and phospholipase A2 activity (53). Downregulation of lipid metabolism and upregulation of glucose metabolism mediated by autophagy is also reported to involve in alveolar repair after bleomycin-induced injury (54), while in another study, inhibition of lipid synthesis was shown to exacerbate bleomycin-induced lung fibrosis (55). These controversial results indicated that the interplay between lipid and glucose metabolisms induced by PM remains not well characterized. The composition of PM pollutants and the exposure times could be potential factors to cause such inconsistency and should be examined in more details.

Overall, we studied the impact of traffic-related PM_1 on lung injury using our previously established rat model for mimicking the dynamic day-to-day exposure on human. We elaborated the lung function and histological changes as well as elucidated the dysregulated molecular mechanisms upon the sub-chronic and chronic exposures of traffic-related PM_1. Although the traffic-related air pollution did not reach a threatening level as suggested by WHO, we observed a significant histological and molecular changes in rats' lungs after three months of traffic-related PM_1 exposure. High levels of oxidative stress and inflammation were confirmed as well. We highlighted dysregulated acute phase response signaling, complement system and intracellular metabolisms as early molecular features in PM_1-exposed rats of which we proposed Serpina3, Atp2a1 and complement proteins as molecular predictors for early PM_1-induced lung injury. After 6-months accumulation of PM_1 exposure, the rats showed significant lung function decline which might be due to the failure in triggering the actin dynamics-related tissue repair mechanisms. Our study utilized rat lung tissues to unravel the pulmonary phenotypes and molecular alterations, however, future study to detect these candidate proteins in the peripheral blood of high-risk human population should be conducted to evaluate their potential as non-invasive biomarker candidates.

Conclusion

Our study systematically explored the phenotypes and pathogenic mechanisms in rat lungs upon sub-chronic and chronic traffic-related PM_1 exposures. The in-depth quantitative tissue proteomics analysis

explored detailed molecular mechanisms involved in the progression of lung injury which eventually led to disturbance of lung functions. According to these findings, we proposed several potential proteins associated with early lung damages in response to traffic-related PM_1 which might be used to screen the subject more susceptible to PM_1 air pollution.

Methods

Chemicals and reagents

Cellytic MT cell lysis reagent, ammonium hydroxide solution, formic acid (FA), triethylammonium bicarbonate (TEABC), and tween-20 were purchased from Sigma-Aldrich (Saint Louis, USA). Trifluoroacetic acid (TFA) were purchased from Wako (Osaka, Japan). Clarity™ Western ECL Substrate and nitrocellulose membranes were purchased from Bio-Rad (California, USA). Acetonitrile (ACN) were purchased from Spectrum (California, USA). Ethylenediaminetetraacetic acid (EDTA) and protease inhibitors were purchased from G-Biosciences (St. Louis, MO, USA). Trypsin was purchased from Promega (Madison, USA). Bicinchoninic acid (BCA) protein assay kit, and Tandem Mass Tag assay (TMT) were purchased from Thermo Fisher Scientific (Rockford, USA). 10% neutral buffered formalin were purchased from CHIN IPAO CO., LTD (Taipei, Taiwan), paraffin was from Leica Microsystems Pty Ltd (Macquarie Park, Australia), and hematoxylin and eosin (H&E) was from Roche Diagnostics (Indianapolis, USA)

Rat model with whole-body exposure to traffic related air pollution (TRAP)

The rat model was previously published in (16) to mimic the TRAP exposure in human. A whole-body exposure system was developed, and the ambient air was continuously sampled by an omnidirectional PM inlet located on the roof of the animal housing followed by exposure into the animal cages. All procedures were performed compliance with the animal and ethics review committee of the Laboratory Animal Center at Taipei Medical University (Taipei, Taiwan).

Each rat was randomly assigned into three groups for exposure within two different periods: (1) three and six months of exposures to whole air from TRAP (3M-PM_1 and 6M-PM_1 groups, respectively); (2) three and six months of exposures to high-efficiency particulate air (HEPA) filtered TRAP (traffic-related gaseous pollutants, shorted as 3M-GAS and 6M-GAS groups, respectively); and (3) three and six months of exposure to conditioned clean air (3M-CTL and 6M-CTL group, respectively). The PM_1 and GAS groups were placed in an urban region nearby a major highway and expressway in New Taipei City, Taiwan. The CTL group was housed in a specific pathogen free I level of Laboratory Animal Center (Taipei, Taiwan).

As indicated in (16), the characteristics of ambient air exposure were continuously monitored. The daily distribution of the geometric mean diameter was 55.8±7.3 (40.3-74.5) nm, and particles were categorized as ultrafine-sized fractions (<100 nm; PM_1) with mass concentration of 16.3±8.2 (4.7-68.8) $\mu g/m^3$. The lung deposition surface area in the alveolar region was 55.1±21.7 (20.7-136.6) mm^2/cm^3. Black carbon

and particle number concentrations were 1800±784 (219-4732) ng/m^3 and 11257±4388 (2218-25733) #/m^3, respectively.

Lung function examination

After the designated time period of exposure, each rat from every group was examined for the lung function by using a Forced Pulmonary Maneuver System (Buxco Research Systems, Wilmington, NC, USA) following the manufacturer's protocols. Briefly, an endotracheal tube was attached to an airway port, and the distal end of the catheter was passed through a small opening located near the airway port. The catheter was then connected to the system. Forced expiratory flow at 25-75% of the pulmonary volume (FEF_{25-75}) and forced expiratory volume at 20 ms (FEV_{20}) were measured. For each test, at least three acceptable measurements were conducted to obtain a reliable mean for all numeric parameters. All procedures were performed under sufficient anesthesia.

Histological evaluation

Lung tissue were collected and washed with ice-cold PBS, followed by fixation with 10% neutral buffered formalin, embedded in paraffin, sectioned, and stained with hematoxylin and eosin (H&E). Histological examinations were conducted under light microscopy by a histopathologist in a blinded manner. The degree of lung injury was scored according to the four criteria: (1) alveolar congestion, (2) hemorrhage, (3) immune cell infiltration, and (4) thickness of the alveolar wall (56). Congestion and thickness of the alveolar wall were graded by a five-points scale as follows: 0 for minimal (little) damage, 1 for mild damage, 2 for moderate damage, 3 for severe damage, and 4 for maximal damage. Hemorrhage was graded as follows: 0 for no red blood cells (RBC) outside of blood vessels, 1 for few interstitial RBC, 2 for few RBC in some alveoli, 3 for moderate number of RBC in some alveoli, 4 for many RBC in most alveoli, 5 for large numbers of RBC in all alveoli. Infiltration of macrophage was graded as follows: 0 for none-rare, 1 for 1-10% of alveoli/saccules contain macrophages, 2 for 10-25%, 3 for 25-75%, 4 for >75% (57).

Tissue lysate collection

Lung tissue from each rat was grounded in liquid nitrogen, collected into an microcentrifuge tube, and lysed with Cellytic MT cell lysis reagent, protease inhibitors, and EDTA in the volume ratio of 98:1:1. The tissue lysate was homogenized by using Minilys® personal homogenizer (Bertin, Rockville, MD, USA) in high speed mode for 15 s twice and the homogenate was centrifuged at 13,000 rpm at 4°C for 10 min to collect the clear supernatant as lung tissue lysate. The lung tissue lysate from each rat was assayed by using BCA protein assay kit to determine the protein concentration.

Gel-assisted digestion, tandem mass tag (TMT) labeling and high pH reversed phage (RP) StageTip fractionation

Fifty micrograms of lung tissue proteins were aliquoted from each of the 5 rats from the 6 exposure groups for our reported gel-assisted digestion with trypsin individually (58). The resulting peptides were

vacuum-dried and resuspended in 100 mM TEABC for BCA protein assay. Ten micrograms of peptides were aliquoted from each of the 5 rats in one exposure group to generate a pooled peptide sample. The pooled peptides from 3M-CTL, 3M-PM_1 and 3M-GAS groups were labeled with TMT126, TMT127 and TMT128 respectively, whereas the 6M-CTL, 6M-PM_1 and 6M-GAS were labeled with TMT129, TMT130 and TMT131 respectively. The TMT-labeled peptides from each group were pooled for RP StageTip fractionation following the protocol in (59). Peptides were eluted sequentially by using 11.1%, 14.5%, 17.4%, 19%, 23%, and 27-80% ACN in ammonium hydroxide solution (pH 11.5). Peptides from each fraction was vacuum-dried and resuspended in 0.1% FA for LC-MS/MS analysis.

NanoLC-nanoESI-MS/MS analysis

NanoLC-nanoESI-MS/MS analysis was performed on a Thermo UltiMate 3000 RSLCnano system connected to a Orbitrap Fusion™ Tribrid™ Mass Spectrometer (Thermo Fisher Scientific, Bremen, Germany) equipped with a nanospray interface (New Objective, Woburn, MA). Peptide mixtures were loaded onto a 75-μm ID, 25-cm PepMap C18 column (Thermo Fisher Scientific) packed with 2 μm particles with a pore width of 100 Å. The peptides were eluted by a 103-min gradient using 5% to 45% mobile phase B (99.9% ACN, 0.1% FA in HPLC-grade water) at a flow rate of 0.4 μL/min. The gradients were slightly adjusted for each RP fraction.

The LC-MS/MS experiments were performed in a data-dependent acquisition mode to sequentially select the top 15 intense precursor ions for higher-energy collision dissociation with the normalized collision energy of 40%. Full MS scans were acquired in orbitrap from *m/z* 300-1,600 with resolution of 120,000 and automated gain control of 400,000 charges or maximum ion time of 50 msec. For MS/MS scans, fragment ions were acquired in Orbitrap with the resolution of 60,000 and automated gain control of 1E5 or max ion time of 100 msec. Precursors with assigned charge states from 2+ to 7+ were included. Previously targeted precursors were dynamically excluded from re-acquisition for 15 s.

Proteome identification and quantification

The LC-MS raw data were searched against SwissProt Rattus norvegicus database (version 2018_11, 8,054 entries) using Mascot implemented in Proteome Discoverer (version 2.2.0.388, Thermo Fisher). The MS and MS/MS tolerances were set to 20 ppm and 0.1 Da, respectively. Tryptic peptides with a maximum of two missed cleavages were allowed. Methylthio (Cys) was set as fixed modification, whereas oxidation (Met), acetylation (protein N-terminal), deamidation (Asn and Gln), and TMT tags (N-terminal, Lys) were set as variable modifications. 1% false discovery rate (FDR) was applied in peptide spectral matches, peptide and protein levels for confident identification. Identified peptides in high confidence with at least 6 amino acids were accepted. For proteome quantification, only unique peptides were included to estimate the protein abundance which was further normalized by the total peptide abundance. Proteins with 1.3-fold changes in abundance (log2 ratio >0.38 or <-0.38) were considered as differentially expressed proteins (DEPs).

Functional analysis

The DEPs from each exposure group were submitted to Ingenuity Pathway Analysis (IPA) (60) for pathway enrichment analysis and Cytoscape (version 3.7.1) with ClueGo (version 2.5.4) plugin (61, 62) for Gene Ontology (GO) analysis (rattus norvegicus database, v.20.05.2019). GO fusion and GO group were selected while other settings remained default. Only the GO terms from biological process, molecular function, and cellular component with lowest term *p*-value (corrected with Bonferroni step down) were included for analysis. For pathway enrichment analysis using IPA, z-scores were obtained for the enriched canonical pathway as well as the disease and biofunction annotations. Annotations with $p<0.05$ were considered significant. A z-score of >0 indicates activation, while <0 indicates inhibition of a cellular function or pathway.

Western blot analysis

Forty µg of protein was run in gel electrophoresis by using 4–20% Mini-PROTEAN® TGX™ Gel (Bio-Rad, CA, USA) followed by protein transfer onto nitrocellulose membranes. After blocking for 1 h at room temperature, the membranes were incubated overnight at 4°C with primary antibodies against Chp1, Serpina3 (1:1000, ABclonal technology, MA, USA), C3, or Vcl (1:1000, both from Santa Cruz, TX, USA), separately. The membranes were thoroughly washed with PBST and then incubated with anti-rabbit or anti-mouse IgG secondary antibody (1:10000, Bioss Antibodies, MA, USA) for 1 h at room temperature. Clarity™ Western ECL Substrate was used to detect the protein bands. Vinculin (Vcl) was used as the loading control and one rat sample from 6M-CTL group was included in each gel as an inter-sample variation control. Quantification of the detected protein bands were quantified by AzureSpot (Azure Biosystems, CA, USA).

Enzyme-linked immunosorbent assay (ELISA)

ELISA approach was adapted to measure 8-isoprostane (Cayman, USA) and IL-6 (R&D System, Minneapolis, MN, USA) in lung tissue lysate, each following the manufacturer's instructions. Data are presented after normalization to the total protein amount.

Statistical analysis

The lung function and lung injury results were reported as the median with interquartile range. Mann-Whitney U test was used to evaluate the significance of difference. Only differences with $p<0.05$ were considered as significant. Statistical analyses were performed by using GraphPad (version 8).

Abbreviations

PM: particulate matter; TRAP: traffic related air pollution; GAS: high-efficiency particulate air-filtered traffic related gaseous pollutants; CTL: clean air control; LC-MS/MS: liquid chromatography tandem mass spectrometry; TMT: tandem mass tag; RP: reversed phase; DEPs: differentially expressed proteins; GO: gene ontology; IPA: ingenuity pathway analysis; ROS: reactive oxygen species; C3: complement 3; Chp1: calcineurin B homologous protein 1; Serpina3: Serine protease inhibitor A3K; IL: interleukin; Atp2a1:

sarcoplasmic/endoplasmic reticulum calcium ATPase 1; Camk2g: calcium/calmodulin-dependent protein kinase type II subunit gamma; Ryr1: ryanodine receptor; Akap5: A-kinase anchor protein 5; Vcl: vinculin; ELISA: enzyme-linked immunosorbent assay; FA: formic acid; ACN: acetonitrile; FDR: false discovery rate; RBC: red blood cells; FEF_{25-75}: forced expiratory flow at 25-75% of the pulmonary volume; FEV_{20}: forced expiratory volume at 20 ms; BCA: bicinchoninic acid.

Declarations

Ethics approval and consent to participate

Animals were treated humanely and all procedures were performed compliance with the animal and ethics review committee of the Laboratory Animal Center at Taipei Medical University (Taipei, Taiwan).

Consent for publication

Not applicable

Availability of data and materials

The datasets used and/or analysed during the current study are available from the corresponding author on reasonable request.

Competing interests

The authors declare that they have no competing interests

Funding

This research is financially supported by the Ministry of Education (Higher Education Sprout Project, DP2-108-21121-01-T-04-03, DP2-109-21121-01-T-01) and Ministry of Science and Technology (MOST108-2113-M-038-004, MOST109-2113-M-038-002) in Taiwan.

Authors' contributions

Y.T.J., D.U.P. and H.C. Chuang conducted the experiments and analyzed the data. K.Y.L., H.C. Chiu and S.Y.W. analyzed and interpreted the data. C.L.H conceived, designed and directed the study, and interpreted the data. Y.T.J., D.U.P. and C.L.H drafted and revised the manuscript. All authors approved the submitted manuscript.

Acknowledgements

Mass spectrometry data were acquired at the Academia Sinica Common Mass Spectrometry Facilities for proteomics and protein modification analysis located at the Institute of Biological Chemistry in Academia Sinica, Taiwan.

References

1. Network GBoDC. Global Burden of Disease Study 2016 (GBD 2016) Results. Institute for Health Metrics and Evaluation (IHME) Seattle, United States; 2017.
2. Nemmar A, Hoet PH, Vanquickenborne B, Dinsdale D, Thomeer M, Hoylaerts MF, et al. Passage of inhaled particles into the blood circulation in humans. Circulation. 2002;105(4):411-4.
3. Li R, Zhou R, Zhang J. Function of PM2.5 in the pathogenesis of lung cancer and chronic airway inflammatory diseases. Oncol Lett. 2018;15(5):7506-14.
4. Yoshizaki K, Brito JM, Silva LF, Lino-Dos-Santos-Franco A, Frias DP, RCR ES, et al. The effects of particulate matter on inflammation of respiratory system: Differences between male and female. Sci Total Environ. 2017;586:284-95.
5. Vignal C, Pichavant M, Alleman LY, Djouina M, Dingreville F, Perdrix E, et al. Effects of urban coarse particles inhalation on oxidative and inflammatory parameters in the mouse lung and colon. Part Fibre Toxicol. 2017;14(1):46.
6. Mei M, Song H, Chen L, Hu B, Bai R, Xu D, et al. Early-life exposure to three size-fractionated ultrafine and fine atmospheric particulates in Beijing exacerbates asthma development in mature mice. Part Fibre Toxicol. 2018;15(1):13.
7. He F, Liao B, Pu J, Li C, Zheng M, Huang L, et al. Exposure to Ambient Particulate Matter Induced COPD in a Rat Model and a Description of the Underlying Mechanism. Sci Rep. 2017;7:45666.
8. Falcon-Rodriguez CI, Osornio-Vargas AR, Sada-Ovalle I, Segura-Medina P. Aeroparticles, Composition, and Lung Diseases. Front Immunol. 2016;7:3.
9. Jeong SC, Cho Y, Song MK, Lee E, Ryu JC. Epidermal growth factor receptor (EGFR)-MAPK-nuclear factor(NF)-kappaB-IL8: A possible mechanism of particulate matter(PM) 2.5-induced lung toxicity. Environ Toxicol. 2017;32(5):1628-36.
10. Gu LZ, Sun H, Chen JH. Histone deacetylases 3 deletion restrains PM2.5-induced mice lung injury by regulating NF-kappaB and TGF-beta/Smad2/3 signaling pathways. Biomed Pharmacother. 2017;85:756-62.
11. Rajagopalan P, Jain AP, Nanjappa V, Patel K, Mangalaparthi KK, Babu N, et al. Proteome-wide changes in primary skin keratinocytes exposed to diesel particulate extract-A role for antioxidants in skin health. J Dermatol Sci. 2018;91(3):239-49.
12. Familari M, Naav A, Erlandsson L, de longh RU, Isaxon C, Strandberg B, et al. Exposure of trophoblast cells to fine particulate matter air pollution leads to growth inhibition, inflammation and ER stress. PLoS One. 2019;14(7):e0218799.
13. Vuong NQ, Breznan D, Goegan P, O'Brien JS, Williams A, Karthikeyan S, et al. In vitro toxicoproteomic analysis of A549 human lung epithelial cells exposed to urban air particulate matter and its water-soluble and insoluble fractions. Part Fibre Toxicol. 2017;14(1):39.
14. Xue ZH, Li A, Zhang XY, Yu WC, Wang JY, Zhang YX, et al. iTRAQ based proteomic analysis of PM2.5 induced lung damage. Rsc Adv. 2019;9(21):11707-17.

15. Araujo JE, Jorge S, Santos HM, Chiechi A, Galstyan A, Lodeiro C, et al. Proteomic changes driven by urban pollution suggest particulate matter as a deregulator of energy metabolism, mitochondrial activity, and oxidative pathways in the rat brain. Sci Total Environ. 2019;687:839-48.
16. Shih CH, Chen JK, Kuo LW, Cho KH, Hsiao TC, Lin ZW, et al. Chronic pulmonary exposure to traffic-related fine particulate matter causes brain impairment in adult rats. Part Fibre Toxicol. 2018;15(1):44.
17. Li Z, Wu Y, Chen HP, Zhu C, Dong L, Wang Y, et al. MTOR Suppresses Environmental Particle-Induced Inflammatory Response in Macrophages. J Immunol. 2018;200(8):2826-34.
18. Wu YF, Li ZY, Dong LL, Li WJ, Wu YP, Wang J, et al. Inactivation of MTOR promotes autophagy-mediated epithelial injury in particulate matter-induced airway inflammation. Autophagy. 2020;16(3):435-50.
19. Persaud L, Zhong X, Alvarado G, Do W, Dejoie J, Zybtseva A, et al. eIF2alpha Phosphorylation Mediates IL24-Induced Apoptosis through Inhibition of Translation. Mol Cancer Res. 2017;15(8):1117-24.
20. Paulin L, Hansel N. Particulate air pollution and impaired lung function. F1000Res. 2016;5.
21. Pope CA, 3rd. Epidemiology of fine particulate air pollution and human health: biologic mechanisms and who's at risk? Environ Health Perspect. 2000;108 Suppl 4:713-23.
22. Leikauf GD, Kim SH, Jang AS. Mechanisms of ultrafine particle-induced respiratory health effects. Exp Mol Med. 2020.
23. Riva DR, Magalhaes CB, Lopes AA, Lancas T, Mauad T, Malm O, et al. Low dose of fine particulate matter (PM2.5) can induce acute oxidative stress, inflammation and pulmonary impairment in healthy mice. Inhal Toxicol. 2011;23(5):257-67.
24. Bhargava A, Shukla A, Bunkar N, Shandilya R, Lodhi L, Kumari R, et al. Exposure to ultrafine particulate matter induces NF-kappabeta mediated epigenetic modifications. Environ Pollut. 2019;252(Pt A):39-50.
25. Carvalho H, Evelson P, Sigaud S, Gonzalez-Flecha B. Mitogen-activated protein kinases modulate H(2)O(2)-induced apoptosis in primary rat alveolar epithelial cells. J Cell Biochem. 2004;92(3):502-13.
26. Radan M, Dianat M, Badavi M, Mard SA, Bayati V, Goudarzi G. In vivo and in vitro evidence for the involvement of Nrf2-antioxidant response element signaling pathway in the inflammation and oxidative stress induced by particulate matter (PM10): the effective role of gallic acid. Free Radic Res. 2019;53(2):210-25.
27. Bosmann M, Ward PA. Role of C3, C5 and anaphylatoxin receptors in acute lung injury and in sepsis. Adv Exp Med Biol. 2012;946:147-59.
28. Ricklin D, Hajishengallis G, Yang K, Lambris JD. Complement: a key system for immune surveillance and homeostasis. Nat Immunol. 2010;11(9):785-97.
29. Hu R, Chen ZF, Yan J, Li QF, Huang Y, Xu H, et al. Complement C5a exacerbates acute lung injury induced through autophagy-mediated alveolar macrophage apoptosis. Cell Death Dis. 2014;5:e1330.

30. Walters DM, Breysse PN, Schofield B, Wills-Karp M. Complement factor 3 mediates particulate matter-induced airway hyperresponsiveness. Am J Respir Cell Mol Biol. 2002;27(4):413-8.
31. Pei L, Zhao M, Xu J, Li A, Luo K, Li R, et al. Associations of ambient fine particulate matter and its constituents with serum complement C3 in a panel study of older adults in China. Environ Pollut. 2019;252(Pt B):1019-25.
32. Braakhuis HM, Park MV, Gosens I, De Jong WH, Cassee FR. Physicochemical characteristics of nanomaterials that affect pulmonary inflammation. Part Fibre Toxicol. 2014;11:18.
33. Hetland RB, Cassee FR, Refsnes M, Schwarze PE, Lag M, Boere AJ, et al. Release of inflammatory cytokines, cell toxicity and apoptosis in epithelial lung cells after exposure to ambient air particles of different size fractions. Toxicol In Vitro. 2004;18(2):203-12.
34. Traboulsi H, Guerrina N, Iu M, Maysinger D, Ariya P, Baglole CJ. Inhaled Pollutants: The Molecular Scene behind Respiratory and Systemic Diseases Associated with Ultrafine Particulate Matter. Int J Mol Sci. 2017;18(2).
35. Clapham DE. Calcium signaling. Cell. 2007;131(6):1047-58.
36. Lee DU, Ji MJ, Kang JY, Kyung SY, Hong JH. Dust particles-induced intracellular Ca(2+) signaling and reactive oxygen species in lung fibroblast cell line MRC5. Korean J Physiol Pharmacol. 2017;21(3):327-34.
37. Deweirdt J, Quignard JF, Crobeddu B, Baeza-Squiban A, Sciare J, Courtois A, et al. Involvement of oxidative stress and calcium signaling in airborne particulate matter - induced damages in human pulmonary artery endothelial cells. Toxicol In Vitro. 2017;45(Pt 3):340-50.
38. Sancini G, Farina F, Battaglia C, Cifola I, Mangano E, Mantecca P, et al. Health risk assessment for air pollutants: alterations in lung and cardiac gene expression in mice exposed to Milano winter fine particulate matter (PM2.5). PLoS One. 2014;9(10):e109685.
39. Ahmad S, Ahmad A, Dremina ES, Sharov VS, Guo X, Jones TN, et al. Bcl-2 suppresses sarcoplasmic/endoplasmic reticulum Ca2+-ATPase expression in cystic fibrosis airways: role in oxidant-mediated cell death. Am J Respir Crit Care Med. 2009;179(9):816-26.
40. Ahmad S, Nichols DP, Strand M, Rancourt RC, Randell SH, White CW, et al. SERCA2 regulates non-CF and CF airway epithelial cell response to ozone. PLoS One. 2011;6(11):e27451.
41. Tong G-Q, Zhang Z-H, Zhao Y, Liu J-J, Han J-B. Traffic-related PM2. 5 induces cytosolic [Ca 2+] increase regulated by Orai1, alters the CaN-NFAT signaling pathway, and affects IL-2 and TNF-α cytoplasmic levels in Jurkat T-cells. Archives of environmental contamination and toxicology. 2015;68(1):31-7.
42. Moe AM, Golding AE, Bement WM. Cell healing: Calcium, repair and regeneration. Semin Cell Dev Biol. 2015;45:18-23.
43. Zhang W, Bhetwal BP, Gunst SJ. Rho kinase collaborates with p21-activated kinase to regulate actin polymerization and contraction in airway smooth muscle. J Physiol. 2018;596(16):3617-35.
44. Zhang W, Huang Y, Gunst SJ. The small GTPase RhoA regulates the contraction of smooth muscle tissues by catalyzing the assembly of cytoskeletal signaling complexes at membrane adhesion sites.

J Biol Chem. 2012;287(41):33996-4008.

45. Chirino YI, Garcia-Cuellar CM, Garcia-Garcia C, Soto-Reyes E, Osornio-Vargas AR, Herrera LA, et al. Airborne particulate matter in vitro exposure induces cytoskeleton remodeling through activation of the ROCK-MYPT1-MLC pathway in A549 epithelial lung cells. Toxicol Lett. 2017;272:29-37.
46. Desai LP, Aryal AM, Ceacareanu B, Hassid A, Waters CM. RhoA and Rac1 are both required for efficient wound closure of airway epithelial cells. Am J Physiol Lung Cell Mol Physiol. 2004;287(6):L1134-44.
47. Southern BD, Grove LM, Rahaman SO, Abraham S, Scheraga RG, Niese KA, et al. Matrix-driven Myosin II Mediates the Pro-fibrotic Fibroblast Phenotype. J Biol Chem. 2016;291(12):6083-95.
48. Wang Y, Zhang M, Li Z, Yue J, Xu M, Zhang Y, et al. Fine particulate matter induces mitochondrial dysfunction and oxidative stress in human SH-SY5Y cells. Chemosphere. 2019;218:577-88.
49. Agarwal AR, Zhao L, Sancheti H, Sundar IK, Rahman I, Cadenas E. Short-term cigarette smoke exposure induces reversible changes in energy metabolism and cellular redox status independent of inflammatory responses in mouse lungs. Am J Physiol Lung Cell Mol Physiol. 2012;303(10):L889-98.
50. Cho SJ, Moon JS, Nikahira K, Yun HS, Harris R, Hong KS, et al. GLUT1-dependent glycolysis regulates exacerbation of fibrosis via AIM2 inflammasome activation. Thorax. 2019.
51. Gong Y, Lan H, Yu Z, Wang M, Wang S, Chen Y, et al. Blockage of glycolysis by targeting PFKFB3 alleviates sepsis-related acute lung injury via suppressing inflammation and apoptosis of alveolar epithelial cells. Biochem Biophys Res Commun. 2017;491(2):522-9.
52. Zhong WJ, Yang HH, Guan XX, Xiong JB, Sun CC, Zhang CY, et al. Inhibition of glycolysis alleviates lipopolysaccharide-induced acute lung injury in a mouse model. J Cell Physiol. 2019;234(4):4641-54.
53. Zhang SY, Shao D, Liu H, Feng J, Feng B, Song X, et al. Metabolomics analysis reveals that benzo[a]pyrene, a component of PM2.5, promotes pulmonary injury by modifying lipid metabolism in a phospholipase A2-dependent manner in vivo and in vitro. Redox Biol. 2017;13:459-69.
54. Li X, Wu J, Sun X, Wu Q, Li Y, Li K, et al. Autophagy Reprograms Alveolar Progenitor Cell Metabolism in Response to Lung Injury. Stem Cell Reports. 2020.
55. Chung KP, Hsu CL, Fan LC, Huang Z, Bhatia D, Chen YJ, et al. Mitofusins regulate lipid metabolism to mediate the development of lung fibrosis. Nat Commun. 2019;10(1):3390.
56. Jiang J-S, Wang L-F, Chou H-C, Chen C-M. Angiotensin-converting enzyme inhibitor captopril attenuates ventilator-induced lung injury in rats. Journal of Applied Physiology. 2007;102(6):2098-103.
57. James ML, Ross AC, Bulger A, Philips JB, Ambalavanan N. Vitamin A and retinoic acid act synergistically to increase lung retinyl esters during normoxia and reduce hyperoxic lung injury in newborn mice. Pediatric research. 2010;67(6):591.
58. Putri DU, Feng PH, Hsu YH, Lee KY, Jiang FW, Kuo LW, et al. Chemotherapy Immunophenoprofiles in Non-Small-Cell Lung Cancer by Personalized Membrane Proteomics. Proteomics Clin Appl. 2018;12(2).

59. Rappsilber J, Mann M, Ishihama Y. Protocol for micro-purification, enrichment, pre-fractionation and storage of peptides for proteomics using StageTips. Nat Protoc. 2007;2(8):1896-906.
60. Krämer A, Green J, Pollard Jr J, Tugendreich S. Causal analysis approaches in ingenuity pathway analysis. Bioinformatics. 2013;30(4):523-30.
61. Shannon P, Markiel A, Ozier O, Baliga NS, Wang JT, Ramage D, et al. Cytoscape: a software environment for integrated models of biomolecular interaction networks. Genome research. 2003;13(11):2498-504.
62. Bindea G, Mlecnik B, Hackl H, Charoentong P, Tosolini M, Kirilovsky A, et al. ClueGO: a Cytoscape plug-in to decipher functionally grouped gene ontology and pathway annotation networks. Bioinformatics. 2009;25(8):1091-3.

Tables

Due to technical limitations Table 1 is available as a download in the Supplementary Files.

Figures

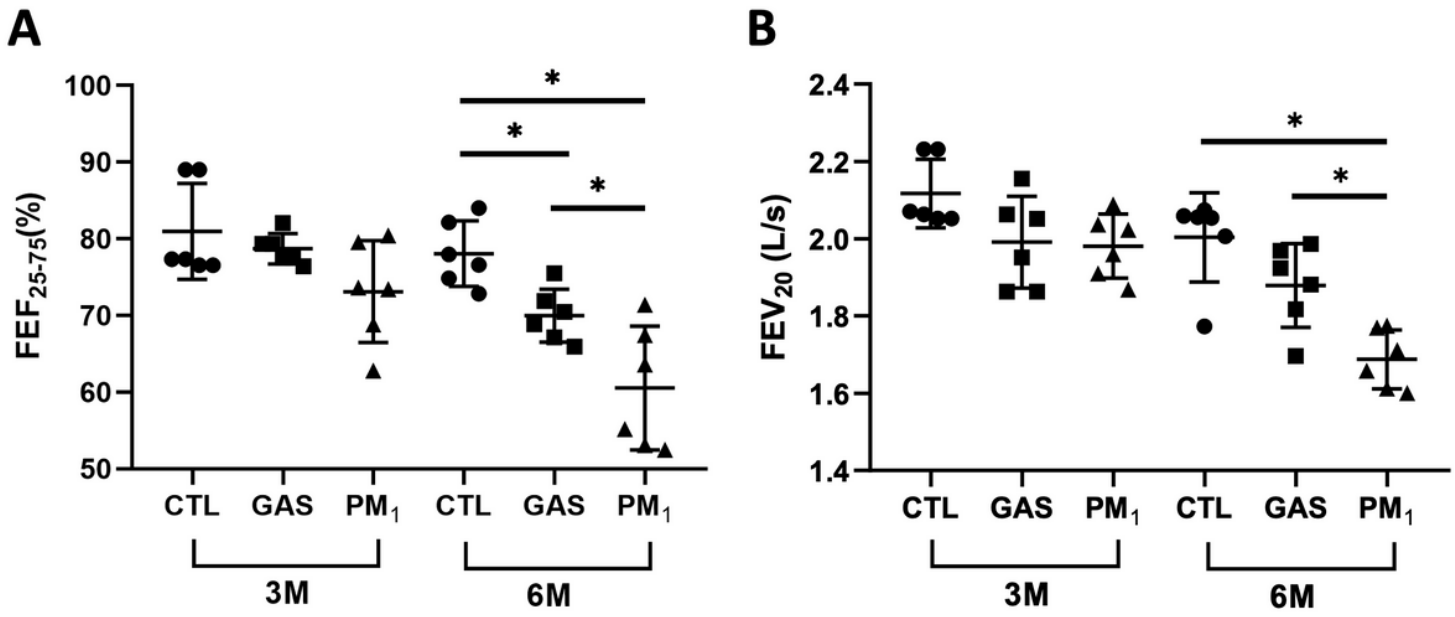

Figure 1

Lung function examination. Forced expiratory flow at 25-75% of the pulmonary volume (FEF25-75) and forced expiratory volume at 20 ms (FEV20) were measured for each rat with at least three acceptable measurements. Significant reduction of FEF25-75 and FEV20 were observed in rats from 6M-PM1 group. * $p<0.05$

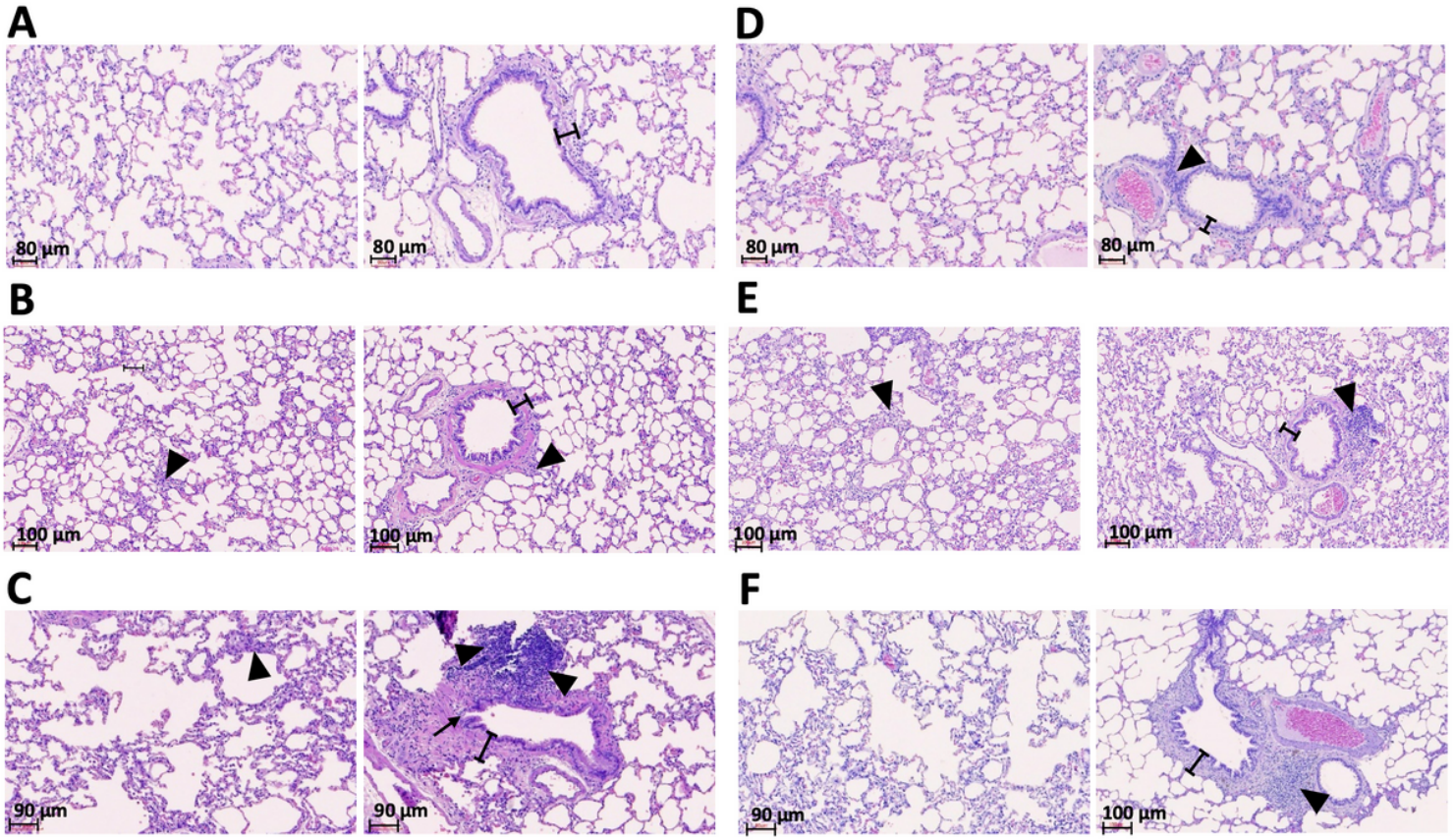

Figure 2

The histological images of rat lung tissues. A, B, and C presented the representative images of 3M-CTL, 3M-GAS and 3M-PM1 groups, while D, E, and F were the representative images of 6M-CTL, 6M-GAS and 6M-PM1 groups, respectively. The images showed the alveoli (left panel) and airway (right panel) tissues. Bars in the airway figures indicate the thickness of airway wall. Black arrowheads point to the infiltration of immune cells within the alveolar and bronchial walls. Black arrow in C indicates damage within the bronchial wall.

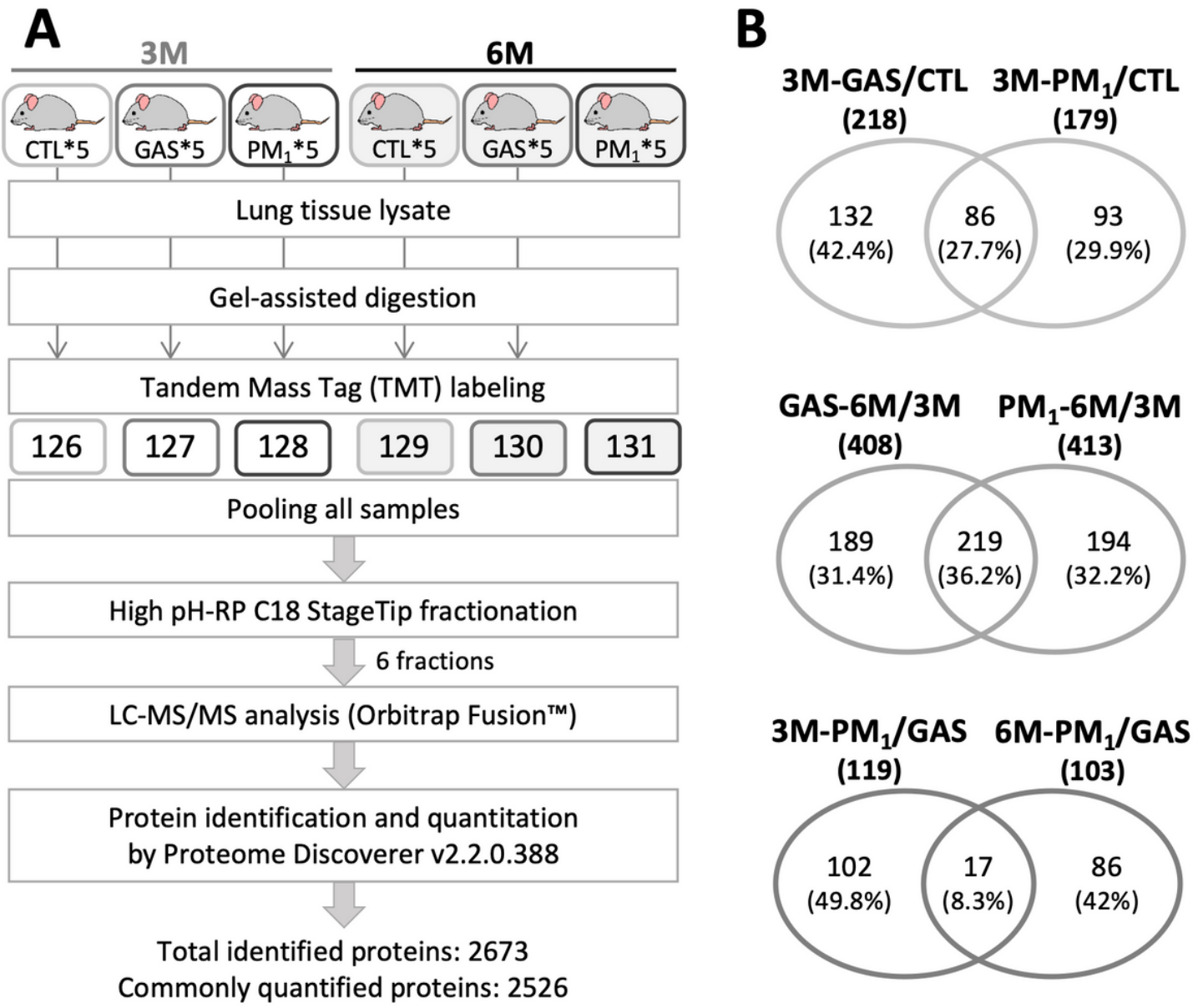

Figure 3

Workflow and differentially expressed proteins (DEPs) for lung tissue proteomics analysis. A The experimental workflow for lung tissue proteomics analysis. The lung tissues from five rats in individual groups were lysed, digested, and pooled to generate six pooled peptide samples. Each pooled sample was labeled with one of the Tandem Mass Tag (TMT) separately. The labeled peptides were then combined for reversed phase C18 StageTip fractionation followed by LC-MS/MS analysis and database searching for protein identification and quantitation. A total of 2673 proteins were identified of which 2526 proteins were quantified. B The overlapping of DEPs in 3M-GAS and 3M-PM1, progressive GAS and PM1 exposures, and the particle-specific DEPs under 3- and 6-month exposures.

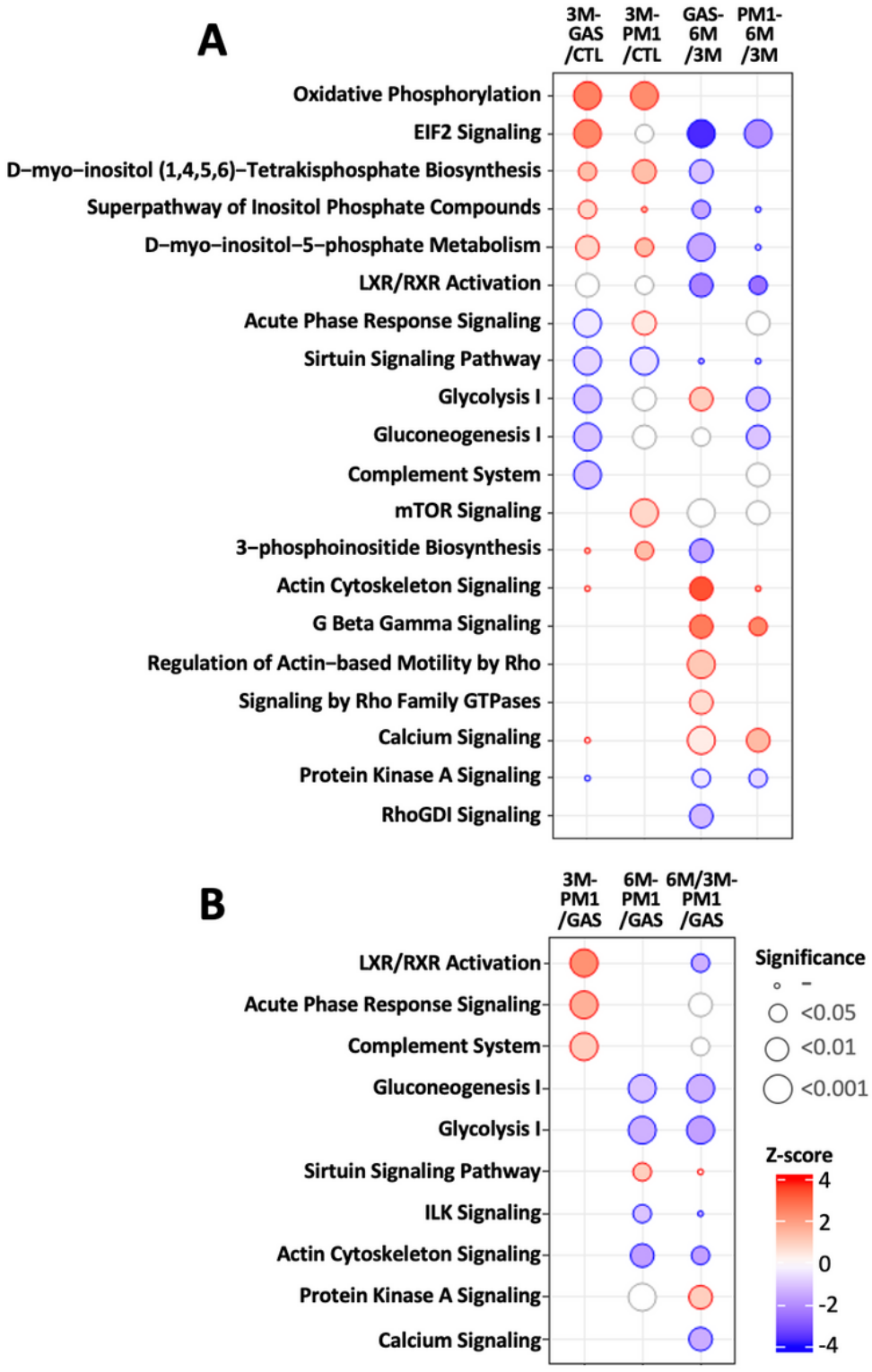

Figure 4

The enriched pathways associated with subchronic and chronic exposures of GAS and PM1. A The enriched pathways associated with subchronic (3-month, two left columns) and progressive exposures of GAS and PM1 (two right columns). B The enriched pathways specifically regulated by the ultrafine-sized particles. The pathway enrichment analysis was performed by using Ingenuity Pathway Analysis (IPA).

The size of the circle represents the p-value for enrichment analysis. The color of the circle indicates activation z-scores; red for up-regulation and blue for down-regulation.

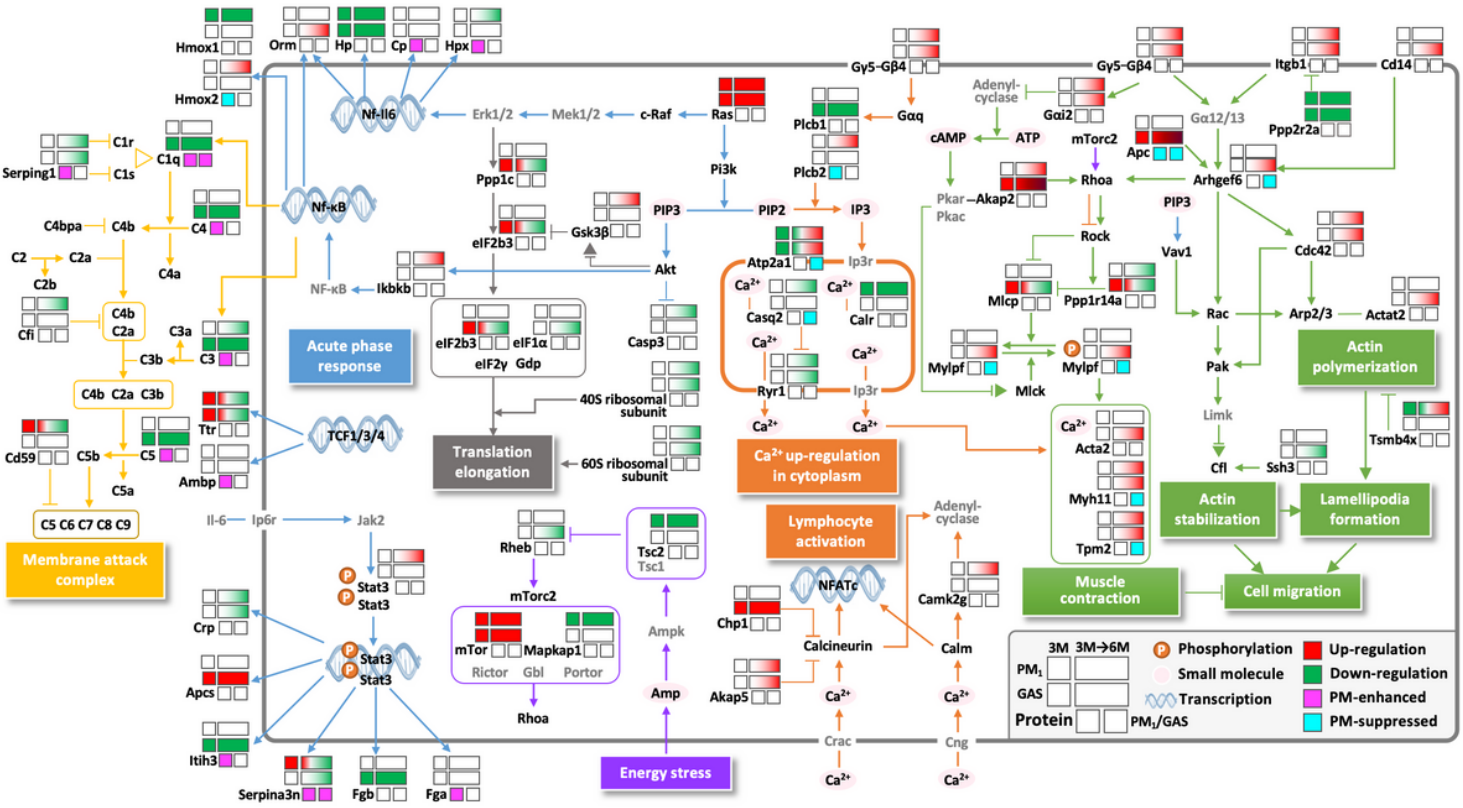

Figure 5

The proposed molecule mechanisms associated with lung injury under sub-chronic and chronic exposure to traffic-related PM1. Boxes on the upper side of the protein gene symbol indicate the protein expression in PM1 (upper) and GAS (lower) groups. Boxes on the left panel of upper side showed the protein ratios in 3M-PM1/CTL and 3M-GAS/CTL, while those on the right panel represented a progression from 3- to 6-month exposures (PM1-6M/3M and GAS-6M/3M, respectively). Upregulated proteins were marked in red, downregulated proteins in green, while unchanged proteins were shown in white color.

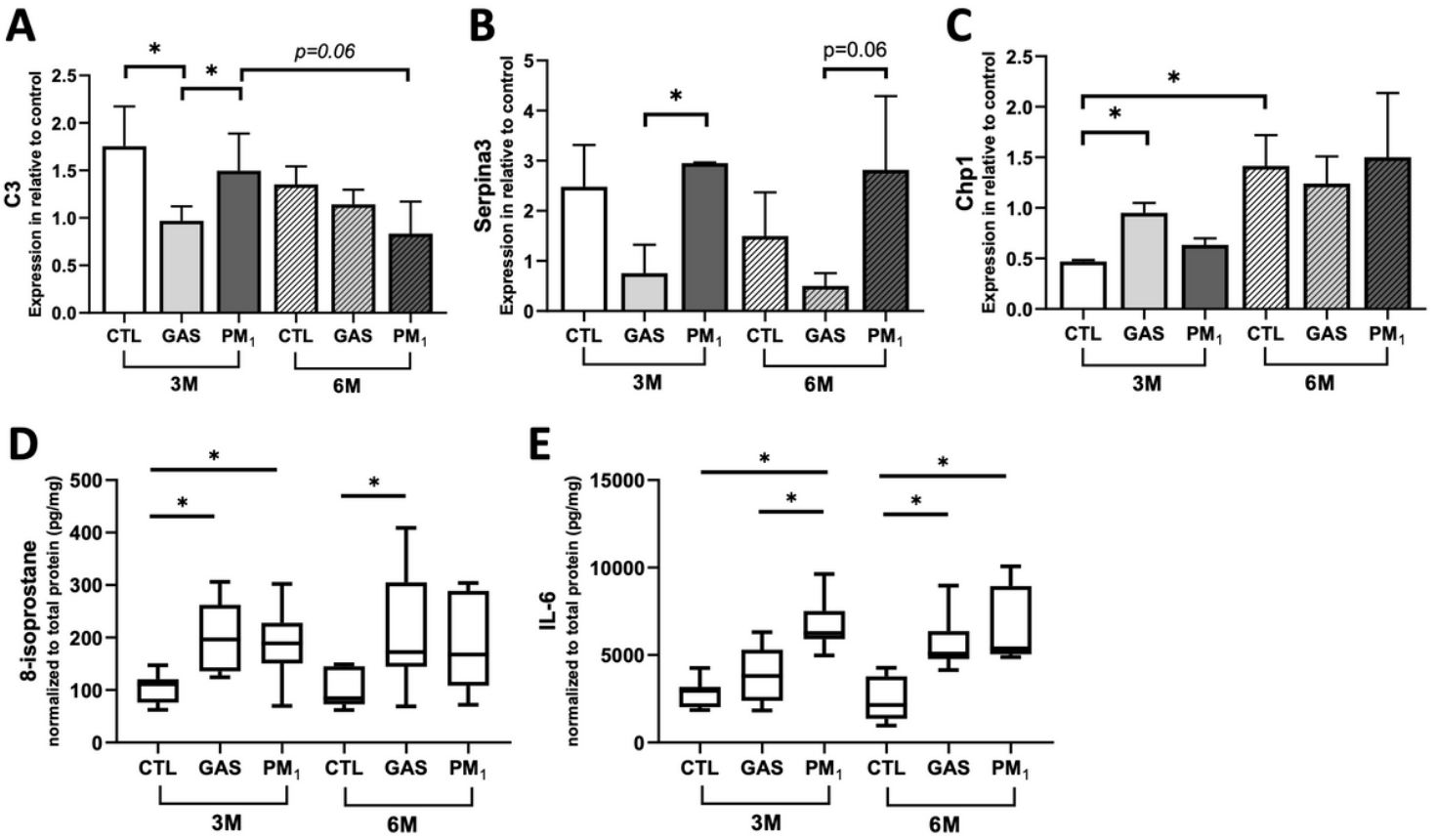

Figure 6

Functional validation of selected proteins, oxidative stress and IL-6 in lung tissues. A, B and C showed the statistical results of western blot analysis of C3, Serpina3, and Chp1 proteins in lung tissues, respectively. The expression of each protein was normalized to the control reference running in every western blot analysis. D and E showed the ELISA results of 8-isoprostane and IL-6, representing the status of oxidative stress and inflammation in lung tissues respectively. The quantities of 8-isoprostane and IL-6 were normalized to total protein lysate before comparison. * $p<0.05$.

Supplementary Files

This is a list of supplementary files associated with this preprint. Click to download.

- Table1.pdf
- OnlineSupplementaryMaterialsall.pdf